SPE 159494

Fluid Characterization Using an EOS for Compositional Simulation of Enhanced Heavy-Oil Recovery

Ashutosh Kumar, SPE and Ryosuke Okuno, SPE, University of Alberta

This paper was prepared for presentation at the SPE Annual Technical Conference and Exhibition held in San Antonio, Texas, USA, 8-10 October 2012.

Abstract

Reliable design of solvent injection for enhanced heavy-oil recovery requires accurate representation of multiphase behavior for heavy-oil/solvent mixtures in a wide range of pressure-temperature-composition conditions. Characterization of a heavy oil is more difficult than that of a conventional oil because the former is conducted under more uncertainties in composition and PVT data. Volume-shift parameters are often required to improve density predictions, separately from compositional behavior predictions, in conventional fluid characterization methods (CM). Thermodynamically, however, volumetric behavior predictions (e.g., densities) are consequences of compositional behavior predictions.

In this paper, we develop a new fluid characterization method (NM) that gives accurate multiphase behavior representation for heavy-oil/solvent mixtures without using volume-shift parameters. The Peng-Robinson (PR) EOS is used with the van der Waals mixing rules. In the NM, pseudo components are initially assigned critical temperature (T_C), critical pressure (P_C), and acentric factor (ω) values that are optimized for the PR EOS for accurate phase behavior predictions for n-alkanes from C_7 to C_{100}. The subsequent regression process searches for an optimum set of T_C, P_C, and ω in physically justified directions. The regression algorithm developed does not require user's experience of thermodynamic modeling for robust convergence. The NM also satisfies Pitzer's definition of ω for each component.

The NM is compared with the CM in terms of various types of phase diagrams, minimum miscibility pressure calculations, and 1-D oil displacement simulations. Twenty two different reservoir oils are used in the comparisons. Results show that the NM with 11 components gives phase behavior predictions that are nearly identical to those using the CM with 30 components. A 1-D simulation case study presents that the NM can robustly reduce dimensionality of composition space while keeping accurate multiphase behavior predictions along composition paths at different dispersion levels tested. We show that the CM with volume shift can give erroneous phase behavior and oil recovery predictions in compositional simulation. The NM does not require volume shift to achieve accurate predictions of compositional and volumetric phase behaviors. The two types of phase behaviors are properly coupled in the NM.

Introduction

Solvent methods for enhanced heavy-oil recovery have been studied and implemented in oil fields (e.g., Mohanty et al. 1995; DeRuiter et al. 1994). Various steam/solvent coinjection schemes are also proposed in the literature to improve efficiency of the conventional steam-assisted gravity drainage (e.g., Hornbrook et al. 1991; Nasr et al. 2003; Gupta et al. 2003; Li et al. 2011; Gates and Chakrabarty 2008). Reliable design of such oil recovery processes requires compositional simulation to model mass transfer among phases using a cubic equation of state (EOS).

Cubic EOSs are widely used in the petroleum industry to model volumetric and compositional phase behavior of conventional oils. The most widely used cubic EOSs are the Peng-Robinson (PR) EOS (Peng and Robinson 1976, 1978) and the Soave-Redlich-Kwong (SRK) EOS (Soave 1972). These EOSs together with the van der Waals mixing rules are suitable for computationally efficient representation of vapor-liquid equilibria for hydrocarbon mixtures at a wide range of pressures (Okuno et al. 2010).

However, application of these EOSs for modeling enhanced heavy-oil recovery is not straightforward. For enhanced recovery of heavy oil, a typical operation range in pressure-temperature-composition (P-T-x) space is much wider than that for enhanced recovery of conventional oil. When steam and solvent are coinjected for heavy-oil recovery, reservoir temperatures lie between an initial reservoir temperature and steam temperatures; e.g., between 290 K and 530 K for a typical solvent-steam-assisted gravity drainage. Also, mixtures of solvent and heavy oils are highly size-asymmetric, resulting in a wider

variety of composition conditions. The wide operation range in P-T-x space provides technical challenges for the traditional use of cubic EOSs with the van der Waals mixing rules.

Fluid characterization using an EOS is conducted based on experimental data available, which typically consist of composition analysis and pressure-volume-temperature (PVT) data. However, it can be difficult to take reliable downhole fluid samples for heavy oil (Zabel et al. 2010; Memon et al. 2010). Even when a reliable sample is available for a heavy oil, its detailed composition is uncertain because of high concentrations of non-identifiable compounds. Availability of experimental data in P-T-x space, especially at different composition conditions, is often limited for heavy oil mainly because of its high viscosity and highly uncertain composition. Heavy-oil PVT data that are easily measurable include saturation pressures (P_{SAT}), densities, and viscosities at different conditions. It is not unusual that they are the only reliable PVT data for a heavy oil.

Characterization of conventional oils using an EOS has been developed, and implemented in commercial software (Whitson and Brulè 2000; Pedersen and Christensen 2007). A typical characterization process consists of four main steps as follows:

Step 1. Estimation of a molar distribution with respect to molecular weight (MW) or carbon number (CN) to split the plus fraction (e.g., C_{7+}) into detailed components.

Step 2. Estimation of properties for the detailed components such as critical temperature (T_C), critical pressure (P_C), critical volume (V_C), acentric factor (ω), and volume-shift parameters.

Step 3. Grouping of the detailed components into fewer pseudo components.

Step 4. Regression of pseudo components' properties to match experimental data available.

In step 1, a distribution function is fitted to the composition analysis data available. Forms of distribution functions proposed in the literature include the gamma (Whitson 1983), chi-square (Quiñones-Cisneros et al. 2003), and logarithmic distributions (Pedersen et al. 1983, 1984). The gamma distribution is the most general form among the three, and reduces to the other two when certain assumptions are used. The logarithmic distribution is a widely used form for conventional oil characterization, where composition analysis can provide composition information for a large fraction of the fluid. Heavy oils often require more flexible distribution functions, like the gamma and chi-square ones, to match their composition analysis data (Ghasemi et al. 2011). Regardless of the type of the distribution function used, however, the reliability of the resulting molar distribution depends primarily on how much uncertainty is left as a plus fraction in composition analysis.

Step 2 uses correlations to estimate properties of the split components because critical properties measured for hydrocarbons heavier than C_{24} are not available (Ambrose and Tsonopoulos 1995). These correlations include Edmister (1958), Cavett (1962), Lee and Kesler (1975), Kesler and Lee (1976), Twu (1984), Riazi and Daubert (1980, 1987), Riazi and Al-Sahaff (1966), and Korsten (2000). The correlations of Pedersen et al. (1989, 1992, 2004) are functions of MW and density at atmospheric conditions, which are in turn functions of CN. These correlations are developed for an EOS to reproduce vapor pressures and the critical point for the pseudo component of a given CN. However, the PR and SRK EOSs with these correlations cannot accurately model densities of heavy hydrocarbons unless volume-shift parameters (Peneloux et al. 1982; Jhaveri and Youngren 1988) are used. Krejbjerg and Pedersen (2006) developed new correlations for T_C, P_C, and ω for heavy-oil characterization. Their correlations do not attempt to model three-hydrocarbon-phase behavior, although such phase behavior often occurs for highly asymmetric mixtures of heavy oil with solvent (Polishuk et al. 2004).

Step 3 reduces the number of components used in the fluid model and calculates properties of each pseudo component by averaging over its member components. Use of fewer components can make EOS calculations more efficient, but it can also result in erroneous predictions of phase behavior due to reduced dimensionality in composition space. Grouping procedures in the literature include the ones of Pedersen et al. (1984) and Whitson and Brulè (2000). The former uses the equal mass grouping with mass-weighted averaging of properties, while the latter uses the equal mole grouping with mole-weighted averaging. As mentioned before, simulation of solvent methods for heavy-oil recovery requires reliable representation of phase behavior at a wide range of composition conditions. Therefore, a reliable fluid model for solvent/heavy-oil mixtures often requires more components than that for solvent/conventional-oil mixtures.

Step 4 is often needed because each of steps 1-3 makes certain assumptions resulting in deviations of predictions from actual phase behavior. Regression procedures for conventional oil characterization are discussed in detail in Whitson and Brulè (2000) and Pedersen and Christensen (2007). Typical parameters adjusted in this step include T_C, P_C, ω, volume-shift parameters, and binary interaction parameters (BIPs) for pseudo components. The constant terms of the attraction and covolume parameters of a cubic EOS, Ω_a and Ω_b, are sometimes adjusted, but this is not recommended as explained by Wang and Pope (2001). These adjustment parameters offer flexibility that may be required to match various types of PVT data such as P_{SAT}, constant mass expansion, constant volume depletion, differential liberation, separator tests, swelling tests, minimum miscibility pressures, and viscosity data. Different EOS fluid models can result depending on which parameters are adjusted and how much they are adjusted (Lolley and Richardson, 1997).

As described above, each of steps 1-4 is more difficult for heavy oil than for conventional oil. The main reason for the difficulties is that heavy-oil characterization is conducted under high uncertainties in oil composition, components' properties (e.g., T_C, P_C, and ω), and phase behavior in P-T-x space. Also, considering direct use of EOS fluid models in compositional simulation, it is undesirable that modeling heavy-oil/solvent mixtures often requires many components to accurately model their phase behavior.

In this research, a new characterization method is developed for simulation of enhanced heavy-oil recovery. We address the uncertainty issues discussed above by incorporating physical observations into our procedures for critical parameter estimation, step 2, and regression, step 4. Since density data are easier to obtain than composition data, especially for heavy oil, our method effectively uses density data to improve phase behavior predictions in P-T-x space; i.e., volume-shift parameters are not required in our characterization method. In the following section, the conventional characterization method used in this research is defined. We then present a new characterization method and its application to 22 different reservoir oils. Comparisons are made between the new and conventional characterization methods in terms of phase behavior predictions in P-T-x space for actual reservoir oils and their mixtures with solvents.

Conventional Characterization Method Used in This Research

The conventional characterization method used in this research is based on Pedersen and Christensen (2007) and the PVTsim software of Calsep (2011). Descriptions are given below for the conventional characterization steps 1-4 (see the introduction section for the definitions of the steps). All characterizations in this research assume that PVT data available are the oil P_{SAT} at the reservoir temperature, and liquid densities and viscosities at different pressures at the reservoir temperature. All EOS calculations in this research use the PR EOS, **Eq. 1,** with the van der Waals mixing rules.

$$p = \frac{RT}{v-b} - \frac{a_c \alpha(T)}{v^2+2bv-b^2}, \tag{1}$$

where $a_c = 0.457235529 \frac{(RT_c)^2}{P_c}$

$$\sqrt{\alpha(T)} = \left[1 + m\left(1 - \left(\frac{T}{T_c}\right)^{0.5}\right)\right]$$

$$m = 0.37464 + 1.54226\omega - 0.26992\omega^2 \quad \text{for } \omega < 0.49 \tag{2}$$

$$m = 0.379642 + 1.48503\omega - 0.164423\omega^2 + 0.016666\omega^3 \quad \text{for } \omega \geq 0.49 \tag{3}$$

Step 1 of the conventional method assumes a logarithmic distribution for splitting a plus fraction. In step 2, critical properties, such as T_C, P_C, and ω, are estimated using Krejbjerg and Pedersen (2006). Step 3 uses the equal mass grouping with mass-weighted averaging of properties.

Although there is no well-defined regression scheme for step 4 due to its high flexibility in the conventional method, **Fig. A.1** depicts the conventional regression scheme used in this research, which is based on Pedersen and Christensen (2007) and Christensen (1999). Adjustments are made for T_C, P_C, and ω of pseudo components to match the P_{SAT} at the reservoir temperature. Adjustment parameters are selected based on their sensitivities to P_{SAT} calculation (Voulgaris et al. 1991).

After matching the P_{SAT}, density data at different pressures at the reservoir temperature are matched. We consider two options here; one is to adjust T_C, P_C, and ω, and the other to adjust volume-shift parameters (the C_{PEN} parameters in the PVTsim software). The second option is widely used in the literature. In this paper, the conventional methods with the first option and with the second option are referred to as the $CM_{w/o}V$ and CM_wV, respectively. The $CM_{w/o}V$ and CM_wV are collectively called the CM. The CM_wV will be compared with our new method (NM) developed in the next section, both with 11 components. The $CM_{w/o}V$ will be used with 30 components to generate pseudo data for the comparisons. In the regression step, we confirm that T_C and P_C have physically correct trends with respect to MW; i.e., T_C monotonically increases and P_C monotonically decreases with increasing MW. As will be discussed, the NM does not require confirming the trends because the physical trends are naturally satisfied.

V_C for pseudo components are also adjusted to match viscosity data using the Lohrenz-Bray-Clark (LBC) model (Lohrenz et al. 1964). BIPs are not adjusted in this research. These two notes also apply for the NM described below.

New Characterization Method Based on Perturbation from n-Alkanes

The new characterization method (NM) developed in this section addresses two major issues that the CM can pose when applied for heavy-oil characterization. These issues, which are described below, come essentially from the fact that heavy-oil characterization must be conducted under high uncertainties in oil composition, components' properties (e.g., T_C, P_C, and ω), and phase behavior in P-T-x space. In the following subsections, we first describe the issues of the CM. Our development of the NW is then presented in detail.

Issues of the Conventional Method

One of the two major issues is in step 2, estimation of pseudo components' properties. Conventional correlations for pseudo components' properties in the literature are typically functions of two parameters; e.g., MW and specific gravity. The fundamental reason for use of two types of parameters is that a CN group contains a wide variety of compounds. One way to categorize hydrocarbon compounds is paraffins, naphthenes, and aromatics (PNA). T_C and P_C of paraffins are in general lower than those of aromatics within a given CN group (Kumar and Okuno 2012). The trend is the other way around for ω. That is, one of the two parameters, specific gravity, is required to consider the effects of a PNA distribution within a CN group on

critical properties of the CN group. However, specific gravities of pseudo components in a plus fraction are unknown. They are then estimated using a function of CN in Pedersen and Christensen (2007). In this way, a certain PNA distribution is implicitly assumed in the CM for property estimation, and the PNA distribution assumed is not well defined for users.

The PNA distribution implicitly set is coupled with a shortcoming of cubic EOSs in the CM. That is, even when T_C, P_C, and ω of a well-defined hydrocarbon (e.g., a n-alkane compound) are given, cubic EOSs are inaccurate in predicting its liquid densities unless a volume-shift parameter is used (Ting et al. 2003; Voutas et al. 2006, Yakoumis et al. 1997). This shortcoming of cubic EOSs is more serious for heavier hydrocarbons (Kumar and Okuno 2012). Regression in step 4 then attempts to decrease errors caused by the coupled problem mentioned above, where adjustments of T_C, P_C, and ω must be performed with little justification in a physical sense.

Another major issue addressed in this research is the separation of volumetric and compositional behaviors using volume-shift parameters in the CM_wV. For heavy oil, available experimental data are mostly volumetric ones, instead of compositional ones. Volume-shift parameters are typically needed when the CM is used with a small number of components to match heavy-oil density data. In such a case, compositional behavior predictions of the resulting fluid model depend significantly on how much one relies on volume-shift parameters to match density data.

Thermodynamically, however, volumetric phase behavior, including densities, is a consequence of compositional phase behavior; i.e., compositional and volumetric phase behaviors should not be modeled separately. Density data for a given fluid contain its composition information. The CM_wV does not effectively use density data to improve compositional phase behavior predictions. Although composition analysis is often difficult for heavy oils, density data can supplement compositional data for heavy-oil characterization by minimizing use of volume-shift parameters. Thus, our NM does not use volume-shift parameters, which can also reduce the number of adjustment parameters.

Characterization Steps in the New Method

The most important novelties of the NM lie in steps 2 and 4 as will be described below. For steps 1 and 3, the NM is based on Quiñones-Cisneros et al. (2003, 2004ab, 2005); i.e., the chi-square distribution is used for step 1, and the equal mass grouping with mass-weighted averaging of properties is used for step 3.

Step 2, estimation of T_C, P_C, and ω for pseudo components, in the NM is based on the correlations of Kumar and Okuno (2012). The PR EOS with the correlations gives accurate predictions of liquid densities and vapor pressures for n-alkanes from C_7 to C_{100} without using volume-shift parameters. The NM considers a PNA distribution of a plus fraction as perturbation from a limiting distribution of 100% n-alkanes. Considering the trends of T_C, P_C, and ω with respect to the PNA distribution, T_C and P_C of a pseudo component should be higher than the n-alkane values from the correlations of Kumar and Okuno (2012). Similarly, ω of a pseudo component should be lower than the n-alkane values. The amounts of perturbations in T_C, P_C, and ω from the n-alkane values are related to the concentration of components other than n-alkanes, especially aromatic components, in the plus fraction. Step 2 of the NM combines the perturbation concept and the correlations of Kumar and Okuno (2012) as given in **Eqs. 4, 5, and 6.**

$$T_c = 508.15 + 688.71\exp\left(-\frac{270.4911}{f_T MW}\right) \quad (4)$$

$$P_c = 537.65\left(\frac{MW}{f_P}\right)^{-0.6296} - 1.58 \quad (5)$$

$$m = 0.51824 + 2.5847(f_m\ MW)^{-\left(\frac{43.4572}{f_m MW}\right)} \quad (6)$$

The m parameter in Eq. 6 is defined in Eqs. 2 and 3 as a one-to-one function of ω. The perturbation factors for T_C, P_C, and m are expressed as f_T, f_P, and f_m, respectively. Equations 4-6 reduce to the correlations of Kumar and Okuno (2012) for n-alkanes when the perturbation factors are 1.0. As a pseudo component deviates from the n-alkane with the same MW, f_T and f_P increase, and f_m decreases from the value of 1.0.

Equations 4-6 also consider another physical trend that can be derived from the correlations of Riazi and Al-Sahhaf (1996) and Pan et al. (1997). Using their correlations, the differences between aromatics and paraffins in terms of T_C and P_C decrease with increasing MW **(Figs. 1 and 2).** In terms of m, the difference exhibits a maximum around MW of 500 gm/mol as shown in **Fig. 3.** These curves indicate that the effects of non-alkane compounds on T_C, P_C, and m vary with MW.

Figures 1-3 also show how T_C, P_C, and m in our Eqs. 4-6 deviate from their n-alkane values as the perturbation factors (f_T, f_P, and f_m) change from unity. Figures 1-3 present that Eqs. 4-6 qualitatively represent the physical trends mentioned above. Fig. 1 shows that the sensitivity of T_C to f_T in Eq. 4 exhibits a maximum around MW of 200 gm/mol, which is not observed from the correlations of Riazi and Al-Sahhaf (1996). However, the behavior of T_C with respect to f_T in the MW range of 100-200 gm/mol does not affect practical fluid characterization because most of pseudo components are out of this MW range, especially for heavy oils.

Step 4 of the NM uses Eqs. 4-6 to regress T_C, P_C, and m of pseudo components for matching P_{SAT} and density data. **Figure A.2** presents the algorithm to adjust f_T, f_P, and f_m. There are three main iteration loops, the P_{SAT}, density, and ω loops. The P_{SAT} loop is the innermost loop contained by the density loop. The ω loop contains the other two loops.

The initial values for f_T and f_P are 1.0. The f_m parameter is initialized by solving **Eq. 7,**

$$0.6 = 0.51824 + 2.5847(f_m MW_1)^{-\left(\frac{43.4572}{f_m\, MW_1}\right)}, \quad (7)$$

where MW_1 is the MW of the lightest pseudo component in a fluid model. The value on the left side of Eq. 7, i.e. 0.6, is lower than the m for benzene, 0.6866 (see Eq. 2 with ω = 0.21). Use of Eq. 7 assumes all pseudo components are heavier than C_6. The value 0.6 can be unduly low if MW_1 is much greater than the MW of benzene. However, this value is recommended for robustness.

In the P_{SAT} loop, f_P is adjusted by Δf_P (e.g., $+10^{-6}$) per iteration to match the P_{SAT} by decreasing the ψ function **(Eq. 8).** Once the ψ function becomes smaller than a tolerance (e.g., 10^{-4}), the density loop decreases the δ function **(Eq. 9)** by adjusting f_T and f_P. In the density loop, f_P is set to 1.0 at the beginning of each iteration, and f_T is adjusted by Δf_T (e.g., $+10^{-5}$) per iteration. If the f_T exceeds 3.5 or the δ function at the current iteration is greater than that at the previous iteration, then the algorithm moves to the ω loop. The f_T value can be greater than the upper bound of 3.5 when MW_1 is much greater than the MW of benzene in Eq. 7.

$$\psi = \frac{\text{abs}(\text{Experimental } P_{SAT} - \text{Calculated } P_{SAT}) * 100}{\text{Experimental } P_{SAT}} \quad (8)$$

$$\delta = \sum_{i=1}^{k} \frac{1}{k} \left[\frac{\text{abs}(\text{Experimental Density} - \text{Calculated Density}) * 100}{\text{Experimental Density}}\right]_i \quad (9)$$

The ω loop is to satisfy the internal consistency of T_C, P_C, and ω; i.e., the definition of ω given by Pitzer (1955) and Pitzer et al. (1955) and in **Eq. 10. Equations 11 and 12** are used to back calculate ω from the current m for each pseudo component. These ω values are then used in Eq. 10 to obtain saturation pressures for pseudo components (P_{SATI}) at $0.7T_C$.

$$(P_{SAT})_{\text{at } T_r = 0.7} = 10^{-(1+\omega)} P_C \quad (10)$$

$$m = 0.37464 + 1.54226\omega - 0.26992\omega^2 \quad \text{for } \omega \le 0.3984 \quad (11)$$

$$m = 0.379642 + 1.48503\omega - 0.164423\omega^2 + 0.016666\omega^3 \quad \text{for } \omega \ge 0.3984 \quad (12)$$

Use of the PR EOS with the current T_C, P_C, and ω yields another saturation pressure at $0.7T_C$ (P_{SATII}) for each pseudo component. The average absolute deviation ε for P_{SATI} and P_{SATII} for all pseudo components is then calculated using **Eq. 13**

$$\varepsilon = \frac{1}{n} \sum_{i=1}^{n} \text{Abs}(P_{SATI} - P_{SATII}), \quad (13)$$

where n is the number of pseudo components. If f_T is greater than 3.5 or the ε function at the current iteration is smaller than that at the previous iteration, f_m is increased by Δf_m (e.g., $+10^{-3}$) to continue on the ω loop. For each ω iteration, f_T and f_P start with 1.0. The final values for f_T, f_P, and f_m are determined when the ε function becomes greater than that at the previous iteration. The final set of f_T, f_P, and f_m gives the first minimum of the ε function encountered in the calculation.

In the regression algorithm, the initial value is 1.0 for f_T and f_P, corresponding to the n-alkane values in Kumar and Okuno (2012). The search direction for f_T and f_P is the increasing direction from their initial values because pseudo components' T_C and P_C should be higher than n-alkane's value for a given MW. So, Δf_T and Δf_P are positive to be physically justified. We set a lower bound for f_m in Eq. 7, which is used as the initial f_m value. So, Δf_m should also be positive. If the converged f_m is smaller 1.0, it is consistent with the ω perturbation concept that pseudo components' ω should be lower than n-alkane's value for a given MW.

The regression algorithm in the NM provides a unique set of T_C, P_C, and m unlike the CM, where the resulting T_C, P_C, and m depend on the selection of adjustment parameters and adjustment amounts for them. Our regression algorithm can work with fewer adjustment parameters, compared to the CM, because of the physical observations incorporated in its development.

Equations 11 and 12 are different from Eqs. 2 and 3 in terms of their ω ranges. Equations 2 and 3 give the same value for m at ω = 0.39839, but not at the boundary ω = 0.49. The value of 0.39839 falls in the ω range 0.20-0.49 that is recommended for both Eqs. 2 and 3 by Peng and Robinson (1978). Therefore, the value of 0.3984 is chosen as the boundary value for Eqs. 11 and 12.

The NM developed in this section uses the PR EOS. However, it can also be used with other cubic EOSs if a new set of critical parameters is developed for the selected cubic EOS as Kumar and Okuno (2012) did for the PR EOS. The regression algorithm assumes that densities, viscosities, and P_{SAT} data are the only available PVT data. More adjustment parameters may be required when more PVT data are available, especially at different composition conditions. The regression algorithm can be extended for such a case by using molar distribution parameters as variables and creating additional loops. For example, the chi-square distribution has two parameters, which influence mole fractions and MWs of pseudo components. These adjustment parameters will be effective especially for heavy oils, considering the importance of molar distributions of pseudo components in EOS calculations. BIPs for pseudo-component/non-hydrocarbon (e.g., CO_2) pairs can significantly affect phase behavior calculations. So, BIPs can also be used as regression parameters. However, we recommend that the regression step should minimize the number of adjustment parameters to avoid physically absurd adjustment of parameters.

Characterization of Reservoir Oils Using the New Method

In this section, the NM is applied to 22 different reservoir oils ranging from 9.5°API to 60.18°API. The oils are actual reservoir oils, for which data are available in the literature as shown in **Table 1.** The number of pseudo components is fixed to be four for the 22 oils. Mole fractions and MWs of pseudo components for oils 1-13 and 18-20 are taken directly from the corresponding references, which are based on the chi-square distribution. P_{SAT} and reservoir temperature data are available in the references as numerical values for the 22 oils. Many of the density data used have been obtained by digitizing density plots in the references. The number of density data points used is given for each oil in Table 1.

Figure 4 shows how the ε function varies with f_m for oils 5, 6, and 9. Step 4 of the NM converges to the final set of f_T, f_P, and f_m (and corresponding T_C, P_C, and *m*) at a minimum ε value for each oil. The same behavior of f_m occurs for the other oils studied in this research.

Table 1 lists the converged f_T, f_P, and f_m values for the 22 oils studied. **Figures 5, 6, and 7** show the relationship between the API gravity and the converged f_T, f_P, and f_m values, respectively. For all the oils, the converged f_T and f_P values are greater than 1.0, and the converged f_m values are smaller than 1.0. These results indicate that the regression algorithm successfully found the solutions that are consistent with the perturbation concept described in the previous section.

Figures 5-7 also show a trend that f_T, f_P, and f_m are converging toward 1.0 as the API gravity becomes larger. This is likely because the paraffinic portion of the PNA distribution for a lighter oil is greater than that for a heavier oil. The PNA distribution of a heavy oil in general can deviate significantly from the reference distribution of 100% n-alkanes because a heavier CN group allows for a wider variety of compounds in it.

Unlike manual adjustments performed in the CM, the regression process in the NM is automatic and takes only 1-3 minutes per oil using our code written in FORTRAN on the Intel Core i7-960 processor at 3.20 GHz and 8.0 GB RAM. The algorithm presented is based on the exhaustive search method of optimization for robustness. More rapid convergence will be achieved if a gradient method is used with initial guesses for f_T, f_P, and f_m based on the previous iteration steps.

Comparisons Between the New and Conventional Methods

We now make comparisons between the NM and CM in terms of various types of phase behavior predictions in P-T-x space for the oils in Table 1. Since there is no data available in composition space for the oils listed in Table 1, pseudo data are created for the 22 oils using the $CM_{w/o}V$ with 30 components (see Fig. A.1 for the $CM_{w/o}V$ algorithm). The 30 components consist of N_2, CO_2, C_1, C_2, C_3, C_4, C_5, C_6, and 22 pseudo components for the C_{7+} fraction. BIPs between the hydrocarbon components are zero. All other BIPs used for the 30-component models are default values in PVTsim as follows: -0.017 for N_2-CO_2, 0.0311 for N_2-C_1, 0.0515 for N_2-C_2, 0.0852 for N_2-C_3, 0.08 for N_2-C_4, 0.1 for N_2-C_5, 0.08 for N_2-C_i, where $i \geq 6$, 0.12 for CO_2,-C_j, where $1 \leq j \leq 6$, and 0.1 for CO_2-pseudo-components.

Separately from the 30-component models created for pseudo data, two fluid models are created for each oil using the NM and CM_wV with 11 components (see Figs. A.1 and A.2 for the CM_wV and NM algorithms, respectively). The 11 components consist of N_2, CO_2, C_1, C_2, C_3, $C_{4\text{-}5}$, C_6, and 4 pseudo components for the C_{7+} fraction. In this research, BIPs are not adjustment parameters, and fixed BIP values are used for the 22 oils. BIPs are zero between the hydrocarbon components. The other BIPs used in the NM are 0.0 for N_2-CO_2, 0.1 for N_2-C_i, where $1 \leq i \leq 6$, 0.13 for N_2-pseudo-components, and 0.1 for CO_2-hydrocarbons. These values are based on Peng and Robinson (1978). BIPs in the CM_wV are default values in PVTsim, which are given above for the 30-component characterization.

In the following subsections, phase behavior predictions based on the NM and CM_wV are compared with the pseudo data. **Tables 2, 3, 4, and 5** give the resulting fluid models for oil 3 (13.38°API) and oil 6 (24.25°API) using the NM and CM_wV. These models are used in many of the comparisons presented below.

P-T Predictions

We first present the comparisons in terms of P-T predictions. Heavy-oil/solvent mixtures often exhibit three hydrocarbon-phases near the vapor pressures of the solvent components. The three phases consist of the gaseous (V), oleic (L_1), and solvent-rich liquid (L_2) phases (e.g., Mohanty et al. 1995; Polishuk et al. 2004). **Figures 8 and 9** show the 2-phase and 3-phase envelopes for a mixture of oil 6 10% and C_2 90%. The CM_wV gives the V-L_1 and V-L_1-L_2 regions that are much smaller than those predicted by the NM. The NM predictions are in good agreement with the pseudo data points. The NM predictions are more accurate for lower temperatures. The three-phase envelope predicted by the NM almost coincides with data.

The deviation of the CM_wV predictions from the pseudo data is more significant for a mixture of oil 6 10% and C_3 90%**.** **Figure 10** shows that the CM_wV results in an erroneous two-phase envelope for this mixture. The NM correctly generates the phase behavior predictions. **Figure 11** shows that the NM predicts a three-phase envelope that is close to the data points. The three-phase behavior predicted by the CM_wV occurs in a much smaller P-T region apart from the correct three-phase region based on the pseudo data and the NM.

The accuracy of the NM for L_1-L_2-V phase behavior is remarkable considering that the complex phase behavior characteristic of highly asymmetric hydrocarbon mixtures is predicted using only four pseudo components for the C_{7+} fraction. The reduced dimensionality in composition space does not damage phase behavior predictions using the NM.

P-x Predictions

A P-x prediction presents a cross section of isothermal phase behavior between two compositions. In this subsection, we show P-x predictions for the oil-6/C_1, oil-6/C_2, and oil-6/CO_2 pairs at the oil-6 reservoir temperature 333.15 K. **Figure 12** shows the P-x predictions along with pseudo data for the oil-6/C_1 pair. The NM and CM_wV are accurate at low mixing ratios of C_1. This is because the 11-component models are fitted to P_{SAT} at the reservoir temperature at the oil composition. As the mixture composition goes away from the oil composition, the CM_wV predictions deviate from the pseudo data. The NM accurately predicts the bubble-point pressures along the mixing line.

The advantage of the NM over the CM_wV becomes more significant for P-x predictions for the oil-6/C_2 pair as shown in **Fig. 13.** At the C_2 mixing ratio of 90%, the CM_wV predicts a bubble point at 137.44 bars, which is approximately 39 bars lower than the pseudo data and the prediction by the NM.

Mixtures of CO_2 and reservoir oil often exhibit continuous transition between L_1-V and L_1-L_2 phase equilibria (Okuno et al. 2011) at low temperatures. **Figure 14** presents such phase behavior for oil 6 and CO_2 at 333.15 K. The NM accurately predicts the upper boundary of the two-phase region in P-x space. The CM_wV erroneously gives a smaller region for the immiscible two liquid phases.

Figure 15 shows saturated liquid densities predicted along the mixing line between oil 6 and the equimolar C_1-C_2 mixture at 333.15 K. The density at the oil composition was used to create the EOS fluid models, so the CM_wV and NM are both accurate at lower mixing ratios of the solvent. As the mixture composition goes away from the oil composition, however, the CM_wV predictions deviate from the NM predictions and the pseudo data. The results indicate that the fluid models based on the CM_wV cannot accurately represent phase equilibria and volumetric properties at compositions away from the oil composition.

T-x Predictions

A T-x diagram presents another important cross section of phase behavior, particularly when coinjection of solvent and steam is considered for heavy-oil recovery. **Figure 16** shows T-x predictions for oil-3/C_6 mixtures at 34.47 bars. The CM_wV overpredicts saturation temperatures except for low C_6 mixing ratios, while the NM accurately predicts them along the mixing line. If the fluid model based on the CM_wV is used in reservoir simulation of solvent/steam coinjection, propagation of the solvent in the reservoir can be significantly underestimated, resulting in erroneous reservoir performance forecasts.

The overprediction of saturation temperatures by the CM_wV becomes more significant for higher pressures. **Figure 17** shows T-x predictions at 60.00 bars. The NM still predicts accurately the saturation temperatures at all mixing ratios tested. However, the CM_wV predicts much higher saturation temperatures even at low C_6 mixing ratios. The deviation at the C_6 mixing ratio of 0.3 is 139 K. At C_6 mixing ratios higher than 0.3, there are no saturation temperatures predicted by CM_wV because the cricondenbar becomes lower than 60.00 bars as can be seen in **Fig. 18.**

Thermodynamic Minimum Miscibility Pressure (MMP) Calculation

The thermodynamic MMP is the minimum displacement pressure at which complete miscibility is developed along the composition path from the injectant to the reservoir oil for one-dimensional flow in the absence of dispersion (Johns and Orr 1996). The thermodynamic MMP is a widely used parameter for design of solvent injection. In this subsection, the thermodynamic MMPs are calculated for 18 oils in Table 1 at their reservoir temperatures. Two different injectants are considered; pure C_1 and pure CO_2. For the C_1 cases, the MMP calculations are performed based on the method of characteristics using PVTsim. For the CO_2 cases, the mixing-cell method within PennPVT (Johns 2012; Ahmadi and Johns 2011) is used. MMP calculations are not shown for oils 1, 2, 4, and 18 because three phases are present during the MMP calculations using the EOS fluid models for these oils based on the $CM_{w/o}V$ with 30 components.

Figure 19 compares the MMPs based on the NM with the pseudo data for 18 oils with C_1. Although the C_1-MMPs presented are calculated at different temperatures, the plots show that the calculated C_1-MMPs are higher for heavier oils. The accuracy of the MMPs observed for the wide variety of oils indicates that the NM successfully retains compositional phase behavior using only four pseudo components for the C_{7+} fraction. **Figure 20** shows that the C_1-MMPs predicted based on the CM_wV are lower than the pseudo data. The deviation is more significant for heavier oils. The maximum deviation of the C_1-MMPs is 5.6% for the NM, but it is 34% for the CM_wV. **Figures 21 and 22** show the comparisons of the NM with the CM_wV in terms of the CO_2-MMP. The maximum deviations of the CO_2-MMPs are 7.4% and 62% for the NM and the CM_wV, respectively.

Figures 20 and 22 indicate that compositional phase behavior predictions are more erroneous for heavier oils using the CM_wV. This is because the CM_wV uses density corrections through volume-shift parameters. A larger amount of volume correction is required and performed for heavier oils in the CM_wV as shown in Tables 3 and 5 (see also the Issues of the Conventional Method subsection). However, the thermodynamic MMP considered here is a parameter representing primarily compositional phase behavior, instead of volumetric phase behavior, of the fluid system considered. Therefore, the separation of volumetric from compositional phase behavior predictions causes errors in MMP predictions.

1-D Displacement Simulation Case Study

Solvent injection for heavy-oil recovery is typically conducted under partially miscible conditions. In such displacements, the oil recovery history depends on how components propagate with the throughput of injectant. This subsection presents a

simulation case study for 1-D isothermal displacement of oil 6 with the equimolar C_1/C_2 mixture under partially miscible conditions. The MMP calculated for this case is 412.23 bars using the $CM_{w/o}V$ with 30 components. Using 11 components, it is 415.38 bars and 327.23 bars based on the NM and the CM_wV, respectively (see Tables 4 and 5 for the fluid models). Input data for the simulations using the GEM simulator of Computer Modelling Group (2011) are given in **Table 6.** The injection and production pressures are fixed at 203.45 bars and 200 bars, respectively. The small pressure difference is used to make pressure variation in the reservoir small. Simulation results based on the $CM_{w/o}V$ with 30 components are used as pseudo data. Simulation results based on the NM and CM_wV are then compared.

Figure 23 shows oil recovery predictions compared to the pseudo data. The recovery curves for 0.0-0.3 hydrocarbon pore-volumes injected (HCPVI) are not shown because they nearly coincide. Oil recovery based on the NM is almost identical to the pseudo data. However, the CM_wV results in oil recovery simulation that is significantly overpredicted by approximately 8%. The overprediction is consistent with other comparisons made in previous subsections, where the fluid models based on the CM_wV exhibit more miscibility in their phase diagrams and MMP calculations. To see the effect of numerical dispersion on oil recovery simulation, the number of gridblocks is decreased from 250 to 50. Figure 23 shows the same advantage of the NM over the CM_wV under more dispersive conditions (The previous subsection showed comparisons for the dispersion-free case). So, the number of gridblocks is fixed to be 250 for further comparisons.

The different oil recovery histories are predicted because the NM and CM_wV predict different saturation profiles as shown in **Fig. 24. Figure 25** shows that the C_1 fronts based on the NM and CM_wV deviate from each other, resulting in different predictions of gas breakthrough as can be seen in Fig. 23. Figure 24 also indicates the CM_wV erroneously predicts faster propagation of heavy components. Since the deviation of the CM_wV shown in Fig. 24 increases with the injectant throughput, the simulation based on the CM_wV becomes more erroneous at later times.

Conclusions

We developed a new method for fluid characterization using the PR EOS with the van der Waals mixing rules. The method characterizes reservoir fluids using perturbations of T_C, P_C, and ω from n-alkane values. T_C, P_C, and ω for n-alkanes used are based on our previous research, which are optimized for the PR EOS for predictions of vapor pressures and liquid densities without volume shift. The optimized reference values allow for robust regression using three perturbation factors f_T, f_P, and f_m for T_C, P_C, and ω, respectively. In our regression, Pitzer's definition of ω is correctly satisfied for each component. The new characterization method was applied to 22 different reservoir oils. Comparisons were made between the new and conventional characterization methods in terms of predictions of various phase diagrams, thermodynamic minimum miscibility pressures (MMPs), and 1-D oil displacement. The conclusions are as follows:

1. The new method (NM) exhibits significant insensitivity of phase behavior predictions to the number of components used for a plus fraction. Two- and three-phase behavior predictions in P-T-x space using the NM with 11 components are almost identical to those using the conventional method without volume shift ($CM_{w/o}V$) with 30 components.
2. The reliability of the NM is also observed for MMP calculations and 1-D oil displacement simulations. Oil displacement predictions based on the NM with 11 components are nearly identical to those based on the $CM_{w/o}V$ with 30 components. This is true even at different dispersion levels tested. Results indicate that the NM can reduce dimensionality of composition space while keeping accurate phase behavior predictions along composition paths at different dispersion levels.
3. The NM does not require volume-shift parameters to accurately predict compositional and volumetric phase behaviors. The conventional method with volume shift (CM_wV) separates volumetric phase behavior predictions from compositional phase behavior predictions. This separation should be carefully used especially for heavy-oil characterization. Our results show that the CM_wV with 11 components yields erroneous phase behavior predictions, which typically show significantly smaller two- and three-phase regions in P-T-x space. The advantage of the NM over the CM_wV in phase behavior predictions is more significant for P-T-x conditions away from those used for parameter regression.
4. The new regression algorithm developed searches for an optimum set of T_C, P_C, and ω for pseudo components using physically justified search directions starting from the well-defined initial values. Unlike in the CM, convergence of T_C, P_C, and ω does not depend on user's experience in thermodynamic modeling. The automatic regression process in the NM took only a few minutes per oil for the 22 oils characterized.
5. The perturbation factors f_T, f_P, and f_m developed in this research are unity for n-alkanes. The perturbation factors capture physical trends that can be derived from the literature; e.g., for a given molecular weight, T_C and P_C are lower and ω is larger for paraffins compared to other types of hydrocarbon compounds. For the 22 oils characterized in this research, the converged f_T and f_P values are all greater than 1.0, and the converged f_m values are all smaller than 1.0. Deviations of f_T, f_P, and f_m from unity can be physically interpreted as deviations of the plus fractions from n-alkane mixtures.
6. The NM requires no changes in the current compositional simulation formulation because it uses the PR EOS with the van der Waals mixing rules.

Nomenclature

Roman Symbols
A = Attraction parameter in a cubic equation of state
A = Aromatic
A_{mix} = Attraction parameter for a mixture in a cubic equation of state
b = Covolume parameter in a cubic equation of state
B_{mix} = Covoulme parameter for a mixture in a cubic equation of state
C_{PEN} = Peneloux volume-shift parameter
m = Parameter in the Peng–Robinson EOS (1978) defined in Eqs. 2 and 3
D = Dimension
f_m = Perturbation factor for the *m* parameter
f_P = Perturbation factor for critical pressure
f_T = Perturbation factor for critical temperature
Δf_m = Step size for f_m
Δf_P = Step size for f_P
Δf_T = Step size for f_T
m_A = Acentric factor for aromatics
k = Number of density data
m_P = Acentric factor for paraffins
n = Number of pseudo components
N = Napthenes
p = Pressure, bar
P = Paraffins
P_C = Critical pressure, bar
P_{CA} = Critical pressure of aromatics, bar
P_{CP} = Critical pressure of paraffins, bar
R = Universal gas constant
T = Temperature, K
T_C = Critical temperature, K
T_{CA} = Critical temperature of aromatics, K
T_{CP} = Critical temperature of paraffins, K
TOL = Tolerance
v = Molar volume, gm/mol
V_C = Critical volume, gm/mol

Abbreviations
^{o}API = API (American Petroleum Institute) gravity
BIP = Binary interaction parameter
CM = Conventional (characterization) method
CM_wV = Conventional (characterization) method using volume shift
$CM_{w/o}V$ = Conventional (characterization) method without using volume shift
CN = Carbon number
EOR = Enhanced oil recovery
EOS = Equation of state
HCPVI = Hydrocarbon pore-volume injected
MMP = Minimum miscibility pressure, bar
MW = Molecular weight, gm/mol
NM = New (characterization) method
PC = Pseudo component
PNA = Paraffin-napthene-aromatic
PR = Peng-Robinson
P-T-x = Pressure-temperature-composition
SRK = Soave-Redlich-Kwong

Greek symbols
δ = Average absolute deviation for density given by Eq. 9
ε = Average absolute deviation for saturation pressure given by Eq. 13

Ω_a = Constant term in the attraction parameter of a cubic EOS
Ω_b = Constant term in the covolume parameter of a cubic EOS
ψ = Absolute % deviation given by Eq. 8
ω = Acentric factor

Acknowledgments

This research was partly funded by a research grant from the Natural Sciences and Engineering Research Council of Canada. Ashutosh Kumar has been awarded a doctoral recruitment scholarship from University of Alberta. We gratefully acknowledge these supports. We also thank Dr. Russell T. Johns for providing the PennPVT software.

References

Ahmadi, K. and Johns, R.T. 2011. Multiple Mixing-Cell Model for MMP Determination, *SPE Journal,* **16**(4): 733-742. SPE-116823-PA.

Ambrose, D., and Tsonopoulos, C., 1995. Vapor-Liquid Critical Properties of Elements and Compounds. 2.Normal Alkanes, *Journal of. Chemical & Engineering Data*, **40**(3): 531-546.

Cavett, R.H., 1962. Physical Data for Distillation Calculations, Vapor-Liquid Equilibria, Proceeding of 27th API Meeting, API Division of Refining, **42**(3): 351-366.

Christensen, P.L., 1999. Regression to Experimental PVT Data, *Journal of Canadian Petroleum Technology*, **38**(13): 1-9.

CMG, 2011. Computer Modeling Group, Calgary, Canada.

Coats, K.H., and Smart, G.T., 1986. Application of a Regression Based EOS PVT Program to Laboratory Data, *SPE Reservoir Engineering*, **1**(3): 277-299.

Cullick, A.S., Pebdani, F.N., and Griewank, A. K., 1989. Modified Corresponding States Method for Predicting Densities of Petroleum Reservoir Fluids, *Industrial & Engineering Chemistry Research*, **28**(3): 340-347.

DeRuiter, R.A., Nash, L.J., and Singletary, M.S. 1994. Solubility and Displacement Behavior of a Viscous Crude With CO_2 and Hydrocarbon Gases, *SPE Reservoir Engineering,* **9**(2): 101-106. SPE-20523-PA.

Edmister, W.C., 1958. Applied Hydrocarbon Thermodynamics, Part 4: Compressibility Factors and Equations of State, *Petroleum Refiner*, **37**(4): 173-179.

Gates, I.D. and Chakrabarty, N. 2008. Design of the Steam and Solvent Injection Strategy in Expanding Solvent Steam-Assisted Gravity Drainage. *Journal of Canadian Petroleum Technology,* **47**(9): 12-20.

Ghasemi, M., Alavian, S.A., and Whitson, C.H., 2011. C_{7+} Characterization of Heavy Oil Based on Crude Assay Data, Presented at SPE Heavy Oil Conference and Exhibition held in Kuwait City, Kuwait, 12-24 December.

Gupta, S., Gittins, S., and Picherack, P. 2003. Insights into Some Key Issues with Solvent Aided Process. *Journal of Canadian Petroleum Technology,* **43**(2): 54-61.

Hornbrook, M.W., Dehghani, K., Qadeer, S., Ostermann, R.D., and Ogbe, D.O. 1991. Effects of CO_2 Addition to Steam on Recovery of West Sak Crude Oil, *SPE Reservoir Engineering,* **6**(3): 278-286. SPE-18753-PA.

Jhaveri, B.S. and Youngren, G.K., 1988. Three Parameter Modification of the Peng-Robinson Equation of State to Improve Volumetric Predictions, *SPE Journal*, **3**(3): 1033-1040.

Johns, R.T. and Orr, Jr., F.M. 1996. Miscible Gas Displacement of Multicomponent Oils. *SPE Journal* **1**(1): 39-50. SPE-30798-PA.

Johns, R.T. 2012. *PennPVT Manual (v. 2.9)*, Gas Flooding Joint Industry Project, EMS Energy Institute, Pennsylvania State University at University Park, PA, USA.

Kesler, M. G. and Lee, B. I., 1976. Improve Prediction of Enthalpy of Fractions, *Hydrocarbon Processing*, **55**(3): 153-158.

Korsten, H., 2000. Internally Consistent Prediction of Vapor Pressure and Related Properties, *Industrial & Engineering Chemistry Research*, **39**(3): 813-820.

Krejbjerg, K. and Pedersen, K. S., 2006. Controlling VLLE Equilibrium with a Cubic EoS in Heavy Oil Modeling, presented at 57th Annual Technical Meeting of the Petroleum Society (Canadian International Petroleum Conference), June 13-15, Calgary, Canada.

Kumar, A., and Okuno, R., 2012, Critical Parameters Optimized for Accurate Phase Behavior Modeling for Heavy n-Alkanes up to C_{100} using the Peng-Robinson Equation of State, submitted to *Fluid Phase Equilibria* on April 22, 2012, under revision.

Lee, B.I. and Kesler, M.G., 1975. A Generalized Thermodynamic Correlation Based on Three- Parameter Corresponding States, *American Institute of Chemical Engineering Journal*, **21**(3): 510-527.

Li, W., Mamora, D.D., and Li. Y. 2011. Solvent-Type and –Ratio Impacts on Solvent-Aided SAGD Process. *SPE Reservoir Evaluation & Engineering,* **14**(3): 320-331. SPE-130802-PA.

Lohrenz, J., Bray, B.G. and Clark, C.R., 1964. Calculating Viscosities of Reservoir Fluids from Their Compositions, *Journal of Petroleum Technology*, **16**(10): 1171-1176.

Lolley, C.S., and Richardson, W.C., 1997. Compositional Input for Thermal Simulation of Heavy Oils with Application to the San Ardo Field, SPE 37538, Presented at International Thermal Operation & Heavy Oil Symposium, Bakersfield, California, 10-12 December.

Memon, A.I., Gao, J., Taylor, S.D., Davies, T.L., Jia, N. 2010. A Systematic Workflow Process for Heavy Oil Characterization. *Journal of Petroleum Technology,* **63**(3): 89-90.

Mohanty, K.K., Masino Jr., W.H., Ma, T.D., and Nash, L.J. 1995. Role of Three-Hydrocarbon-Phase Flow in a Gas-Displacement Process. *SPE Reservoir Engineering,* **10**(3): 214-221. SPE-24115-PA

Nasr, T.N., Beaulieu, G., Golbeck, H., and Heck, G. 2003. Novel Expanding Solvent-SAGD Process "ES-SAGD". *Journal of Canadian Petroleum Technology,* **42**(1): 13-16.

Okuno, R., Johns, R.T., and Sepehrnoori, K. 2010. Three-Phase Flash in Compositional Simulation Using a Reduced Method. *SPE Journal,* **15**(3): 689-703. SPE-125226-PA.

Okuno, R., Johns, R.T., and Sepehrnoori, K. 2011. Mechanisms for High Displacement Efficiency of Low-Temperature CO_2 Floods. *SPE Journal,* **16**(4): 751-767. SPE-129846-PA.

Pan, H., Firoozabadi, A., and Fotland, E, 1997. Pressure and Composition Effect on Wax Precipitation: Experimental Data and Model Results, *SPE Production & Facilities*, **12**(4): 250-258.

Pedersen, K. S., Milter, J., and Sørensen, H., 2004. Cubic Equations of State Applied to HT/HP and Highly Aromatic Fluids, *SPE Journal*, **9**(2): 186-192.

Pedersen, K.S., Blilie, A.L., and Meisingset, K.K., 1992. PVT Calculations on Petroleum Reservoir Fluids Using Measured and Estimated Compositional Data for the Plus Fraction, *Industrial & Engineering Chemistry Research*, **31**(5): 1378-1384.

Pedersen, K.S., and Christensen, P.L., 2007, Phase Behavior of Petroleum Reservoir Fluids, CRC Press, Taylor & Francis Group, Boca Raton, FL, USA

Pedersen, K.S., Thomassen, P. and Fredenslund, Aa., 1989. Characterization of Gas Condensate Mixtures, *Advances in Thermodynamics*, Taylor & Francis, New York, 1, 137-152.

Pedersen, K.S., Thomassen, P., and Fredenslund, Aa., 1983. SRK-EOS Calculation for Crude Oils, *Fluid Phase Equilibria*, **14**(C): 209–218.

Pedersen, K.S., Thomassen, P., and Fredenslund, Aa., 1984. Thermodynamics of Petroleum Mixtures Containing Heavy Hydrocarbons. 1. Phase Envelope Calculations by Use of the Soave-Redlich-Kwong Equation of State, *Industrial & Engineering Chemistry Process Design and Development*, **23**(1): 163–170.

Peneloux, A., Rauzy, E. and Fréze, R., 1982. A Consistent Correlation for Redlich-Kwong-Soave Volumes, *Fluid Phase Equilibria*, **8**(1): 7-23.

Peng, D.-Y. and Robinson, D.B., 1976. A New Two-Constant Equation of State, *Industrial & Engineering Chemistry Fundamentals*, **15**(1): 59-64.

Peng, D.-Y., and Robinson, D.B., 1978. The Characterization of the Heptanes and Heavier Fractions for the GPA Peng-Robinson Programs, GPA Research Report RR-28.

Pitzer, K.S, 1955. The Volumetric and Thermodynamic Properties of Fluids. I. Theoretical Basis and Viral Coefficients, *Journal of American Chemical Society*, **77**(13): 3427- 3433.

Pitzer, K.S., Lippmann, D.Z., Curl, Jr. R. F., Huggins, C.M., and Petersen, D.E., 1955. The Volumetric and Thermodynamic Properties of Fluids. II. Compressibility Factor, Vapor Pressure and Entropy of Vaporization, *Journal of American Chemical Society*, **77**(13): 3433-3440.

Polishuk, I., Wisniak, J., and Segura, H. 2004. Estimation of Liquid-Liquid-Vapor Equilibria in Binary Mixtures of n-Alkanes. *Industrial and Engineering Chemistry Research,* **43**(18): 5957-5964.

PVTsim, 20.0, 2011. CALSEP International Consultants, Copenhagen, Denmark.

Quiñones-Cisneros, S.E., Andersen, S.I., and Creek, J., 2005. Density and Viscosity Modeling and Characterization of Heavy Oils, *Energy & Fuels*, **19**(4): 1314-1318.

Quiñones-Cisneros, S.E., Zéberg-Mikkelsen, C.K., Baylaucq, A., and Boned, C., 2004a. Viscosity Modeling and Prediction of Reservoir Fluids: From Natural Gas to Heavy Oils, *International Journal of Thermophysics*, **25**(5): 1353-1366.

Quiñones-Cisneros, S.E., Dalberg, A., and Stenby, E.H., 2004b. PVT Characterization and Viscosity Modeling and Prediction of Crude Oils," *Petroleum Science and Technology*, **22**(9-10): 1309–1325.

Quiñones-Cisneros, S.E., Zéberg-Mikkelsen, C.K., and Stenby, E.H., 2003. Friction Theory Prediction of Crude Oil Viscosity at Reservoir Conditions Based on Dead Oil Properties, *Fluid Phase Equilibria*, **212**(1-2): 233–243.

Riazi, M.R. and Daubert, T.E., 1980. Simplify Property Predictions, *Hydrocarbon Processing*, **59**(3): 115-116.

Riazi, M.R. and Daubert, T.E., 1987. Characterization Parameters for Petroleum Fractions, *Industrial & Engineering Chemistry Research*, **26**(4): 755-759.

Riazi, M.R., and Al-Sahhaf, T.A., 1996. Physical Properties of Heavy Petroleum Fractions and Crude Oils, *Fluid Phase Equilibria*, **117**(1-2): 217-224.

Soave, G., 1972. Equilibrium Constants from a Modified Redlich-Kwong Equation of State, *Chemical Engineering Science*, **27**(6): 1197-1203.

Ting, P.D., Joyce, P.C., Jog, P.K., Chapman, W.G., and Thies, M.C., 2003. Phase Equilibrium Modeling of Mixtures of Long-chain and Short Chain Alkanes Using Peng-Robinson and SAFT, *Fluid Phase Equilibria*, **206**(1-2): 267-286.

Twu, C.H., 1984. An Internally Consistent Correlation for Predicting the Critical Properties and Molecular Weights of Petroleum and Coal-Tar Liquids, *Fluid Phase Equilibria*, **16**(2): 137-150.

Voutsas, E.C., Pappa, G.D., Magoulas, K., and Tassios, D.P., 2006. Vapor Liquid Equilibrium Modeling of Alkane Systems with Equation of State: "Simplicity versus Complexity", *Fluid Phase Equilibria*, **240**(2): 127-139.

Voulgaris, M., Stamatakis, S., Magoulas, K., and Tassios, D., 1991. Prediction of Physical Properties for Non-polar Compounds, Petroleum and Coal Liquid Fractions, *Fluid Phase Equilibria*, **64**, 73-106.

Yakoumis, I. Kontogeorgis, G.M., Voutsas, E., and Tassios, D. 1997. Vapor-Liquid Equilibria for Alcohol/Hydrocarbon Systems Using the CPA Equation of State. *Fluid Phase Equilibria,* **130**(1-2): 31-47.

Wang, P. and Pope, G.A. 2001. Proper Use of Equations of State for Compositional Reservoir Simulation. *Journal of Petroleum Technology,* **53**(7): 74-81.

Whitson, C.H., 1983. Characterizing Hydrocarbon Plus Fractions, *SPE Journal*, **23**(4), 683-694.

Whitson, C.H. and Brulè, M.R., 2000. Phase Behaviour, SPE Henry L. Doherty Series, Vol. 20, Soc. Petrol. Engs. Inc., Richardson, Texas.

Zabel, F., Law, D.H.-S., Taylor, S., and Zuo, J. 2010. Impact of Uncertainty of Heavy Oil Fluid Property Measurements. *Journal of Canadian Petroleum Technology,* **49**(3): 28-35.

Table 1. Twenty two reservoir oils characterized in this research and converged f_T, f_P, and f_m values using the new characterization method

Oil No.	References	MW (gm/mol)	°API	Reservoir Temperature (K)	No. of Density Data (k in Eq. 9)	f_T	f_P	f_m
1	Quiñones-Cisneros et al. (2005), Oil-8	443.08	9.50	322.05	13	2.17147	1.73400	0.359
2	Quiñones-Cisneros et al. (2005), Oil-7	431.59	11.63	322.05	12	1.75256	1.64495	0.368
3	Quiñones-Cisneros et al. (2004a), Oil-6	377.88	13.38	322.05	13	2.97104	1.82457	0.246
4	Quiñones-Cisneros et al. (2004a), Oil-5	422.94	11.98	322.05	13	1.86036	1.65916	0.379
5	Quiñones-Cisneros et al. (2004a), Oil-1	170.59	20.81	330.40	16	3.02971	1.78694	0.406
6	Quiñones-Cisneros et al. (2004b), Oil-8	182.05	24.25	333.15	16	2.93681	1.91583	0.429
7	Quiñones-Cisneros et al. (2004b), Oil-7	159.99	29.24	330.40	16	2.38392	1.74502	0.440
8	Quiñones-Cisneros et al. (2004b), Oil-6	118.18	35.61	346.15	5	2.13263	1.71679	0.434
9	Quiñones-Cisneros et al. (2004b), Oil-5	130.55	28.30	337.85	3	2.99111	1.85084	0.453
10	Quiñones-Cisneros et al. (2004b), Oil-4	114.57	33.35	337.85	6	2.53622	1.74607	0.493
11	Quiñones-Cisneros et al. (2004b), Oil-3	87.80	40.46	337.25	5	2.42193	1.65192	0.554
12	Quiñones-Cisneros et al. (2004b), Oil-2	89.83	47.63	366.45	11	2.15660	1.47331	0.540
13	Quiñones-Cisneros et al. (2004b), Oil-1	86.57	60.18	427.60	13	1.43504	1.18242	0.642
14	Oil*	296.90	22.60‡	357.50	13	2.31403	1.62078	0.309
15	Coats and Smart (1986), Oil-1	123.79	34.04	355.37	8	2.71743	1.85304	0.402
16	Coats and Smart (1986), Oil-6	83.31	55.73	385.37	20	2.14293	1.45227	0.453
17	Coats and Smart (1986), Oil-7	113.60	47.09	328.15	20	1.97029	1.46148	0.499
18	Quiñones-Cisneros et al. (2003), Oil-5	240.24	20.19	345.93	15	1.57415	1.56712	0.585
19	Quiñones-Cisneros et al. (2003), Oil-4	167.03	25.70	344.95	11	2.15396	1.67997	0.588
20	Quiñones-Cisneros et al. (2003), Oil-3	114.65	34.24	337.85	12	2.08488	1.60514	0.616
21	Cullick et al. (1992), Light Oil	105.28	43.68	377.59	8	2.11704	1.56141	0.414
22	Pedersen et a. (1992), Fluid-1	124.57	35.73	344.75	8	1.91030	1.54935	0.615

*This is an actual oil, but the source is not mentioned for confidentiality.
‡As reported. All other densities are calculated values.

Table 2. Fluid model for oil 3 developed using the new characterization method with 11 components.

Components	Mole Fractions	MW (gm/mol)	T_C (K)	P_C (bars)	V_C (cc/mol)	ω
N_2	0.0004	28.02	126.20	33.90	89.80	0.0400
CO_2	0.0216	44.01	304.20	73.80	94.00	0.2250
C_1	0.1992	16.04	190.60	46.00	99.00	0.0080
C_2	0.0011	30.07	305.40	48.84	148.00	0.0980
C_3	0.0002	44.10	369.80	42.46	203.00	0.1520
C_{4-5}	0.0010	67.94	453.70	35.12	283.50	0.2357
C_6	0.0021	86.18	508.00	30.31	370.00	0.3005
PC1	0.3389	275.45	1003.02	21.25	805.80	0.2133
PC2	0.2015	463.51	1074.04	14.88	1951.96	0.3962
PC3	0.1430	652.65	1107.19	11.68	3834.48	0.5671
PC4	0.0910	1025.86	1138.37	8.40	7984.38	0.8356
Temperature (K)		322.05				
Saturation Pressure (bars)		47.23				

Table 3. Fluid model for oil 3 developed using the conventional characterization method with volume shift with 11 components.

Components	Mole Fractions	MW (gm/mol)	T_C (K)	P_C (bars)	V_C (cc/mol)	ω	C_{PEN} (cc/mol)
N_2	0.0004	28.02	126.20	33.90	89.80	0.0400	-4.23
CO_2	0.0216	44.01	304.20	73.80	94.00	0.2250	-1.64
C_1	0.1992	16.04	190.60	46.00	99.00	0.0080	-5.20
C_2	0.0011	30.07	305.40	48.84	148.00	0.0980	-5.79
C_3	0.0002	44.10	369.80	42.46	203.00	0.1520	-6.35
C_{4-5}	0.0010	67.94	453.70	35.12	283.50	0.2355	-5.53
C_6	0.0021	86.18	508.00	30.31	370.00	0.3004	1.39
PC1	0.4294	226.26	702.850	21.56	1212.59	0.3701	-96.76
PC2	0.1744	532.79	803.872	17.25	2357.30	0.4100	-405.20
PC3	0.1072	853.44	860.001	15.76	3754.90	0.4257	-753.83
PC4	0.0632	1450.93	841.495	14.80	6744.42	0.4330	-1458.94
Temperature (K)		322.05					
Saturation Pressure (bars)		47.23					

Table 4. Fluid model for oil 6 developed using the new characterization method with 11 components.

Components	Mole Fractions	MW (gm/mol)	T_C (K)	P_C (bars)	V_C (cc/mol)	ω
N_2	0.0002	28.02	126.20	33.90	89.80	0.0400
CO_2	0.0096	44.01	304.20	73.80	94.00	0.2250
C_1	0.3203	16.04	190.60	46.00	99.00	0.0080
C_2	0.0349	30.07	305.40	48.84	148.00	0.0980
C_3	0.0039	44.10	369.80	42.46	203.00	0.1520
C_{4-5}	0.0120	64.08	440.95	36.27	283.50	0.2215
C_6	0.0053	86.18	508.00	30.31	370.00	0.3005
PC1	0.2472	175.93	916.16	29.65	358.28	0.2423
PC2	0.1640	265.30	994.85	22.53	867.89	0.3953
PC3	0.1217	357.55	1040.46	18.40	1704.91	0.5423
PC4	0.0810	537.28	1088.36	13.88	3550.06	0.7793
Temperature (K)		333.15				
Saturation Pressure (bars)		137.8				

Table 5. Fluid model for oil 6 developed using the conventional characterization method with volume shift with 11 components.

Components	Mole Fractions	MW (gm/mol)	T_C (K)	P_C (bars)	V_C (cc/mol)	ω	C_{PEN} (cc/mol)
N_2	0.0002	28.02	126.20	33.90	89.80	0.0400	-4.23
CO_2	0.0096	44.01	304.20	73.80	94.00	0.2250	-1.64
C_1	0.3203	16.04	190.60	46.00	99.00	0.0080	-5.20
C_2	0.0349	30.07	305.40	48.84	148.00	0.0980	-5.79
C_3	0.0039	44.10	369.80	42.46	203.00	0.1520	-6.35
C_{4-5}	0.0120	64.08	440.95	36.27	283.50	0.2217	-5.91
C_6	0.0053	86.18	508.00	30.31	370.00	0.3005	1.39
PC1	0.2472	147.787	744.734	29.24	693.47	0.3917	-5.91
PC2	0.1640	289.608	871.316	23.07	1142.91	0.4496	-18.45
PC3	0.1217	449.077	944.574	20.15	1732.70	0.5371	-66.56
PC4	0.0810	759.664	1034.300	18.04	3134.73	0.5307	-130.90
Temperature (K)		333.15					
Saturation Pressure (bars)		137.8					

Table 6. Input parameters used in the 1-D simulation case study

No. of gridblocks	250	Reservoir pressure	200 bars
Grid dimensions	3.05 m x 3.05 m x 1.52 m	Reservoir temperature	333.15 K
Permeability	1500 mD	Production pressure	200 bars
Porosity	0.15	Injection pressure	203.45 bars
Initial oil saturation	0.8		
Initial water saturation	0.2	Injection gas	CH_4:C_2H_6 (50:50)

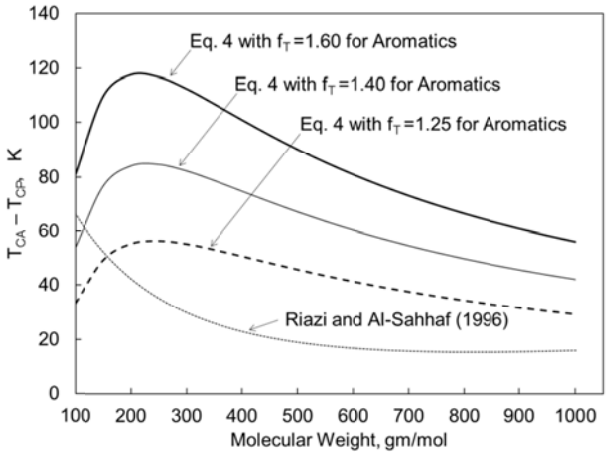

Figure 1. Differences between aromatics and paraffins for critical temperature, T_{CA}-T_{CP}, based on the correlations of Riazi and Al-Sahhaf (1996) and Eq. 4. T_{CA} using Eq. 4 assumes three different f_T values for aromatics, 1.25, 1.40, and 1.60. T_{CP} using Eq. 4 uses f_T of 1.0.

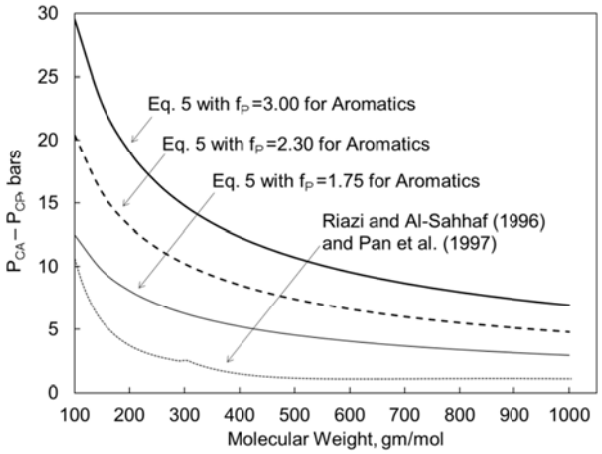

Figure 2. Differences between aromatics and paraffins for critical pressure, P_{CA}-P_{CP}, based on the correlations of Riazi and Al-Sahhaf (1996), Pan et al. (1997), and Eq. 5. P_{CA} using Eq. 5 assumes three different f_P values for aromatics, 1.75, 2.30, and 3.0. P_{CP} using Eq. 5 uses f_P of 1.0. The correlation of Pan et al. (1997) is used for molecular weight larger than 300 gm/mol.

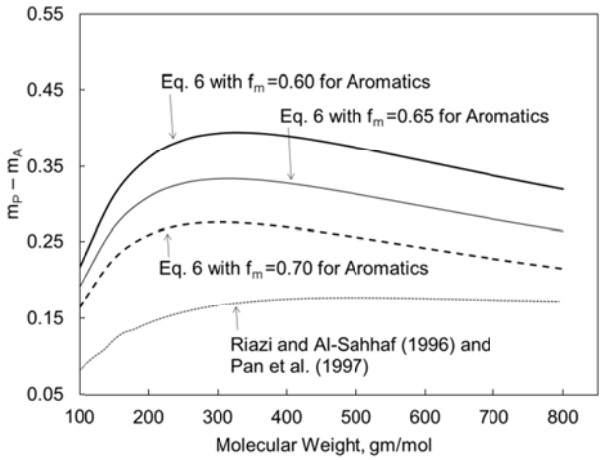

Figure 3. Differences between aromatics and paraffins for the m parameter, m_P-m_A, based on the correlations of Riazi and Al-Sahhaf (1996), Pan et al. (1997), and Eq. 6. The m parameter is defined in Eqs. 2 and 3. m_A using Eq. 6 assumes three different f_m values for aromatics, 0.60, 0.65, and 0.70. m_P using Eq. 6 uses f_m of 1.0. The correlation of Riazi and Al-Sahhaf (1996) is used for m_P, and the correlation of Pan et al. (1997) is used for m_A.

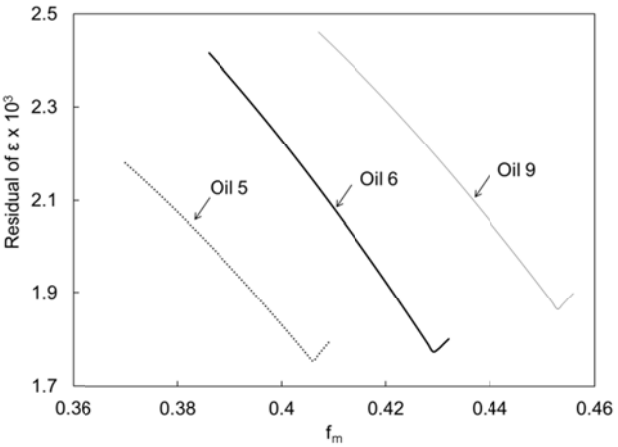

Figure 4. Convergence behavior for the ε function (Eq. 13) with f_m for oils 5, 6, and 9 given in Table 1. The regression algorithm (Fig. A.2) finds an optimum set of f_T, f_P, and f_m at the minimum shown for each oil.

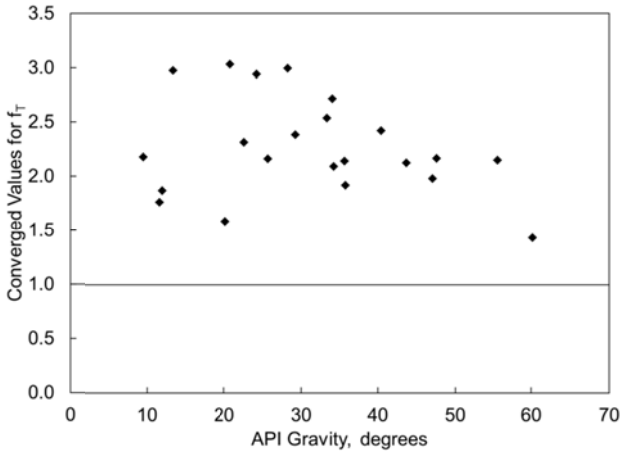

Figure 5. The converged f_T values for the 22 different oils in Table 1. The regression algorithm (Fig. A.2) starts with f_T =1.0, and searches for an optimum f_T in the increasing direction. Perturbation of f_T from 1.0 qualitatively represents deviation of a plus fraction from a n-alkane mixture.

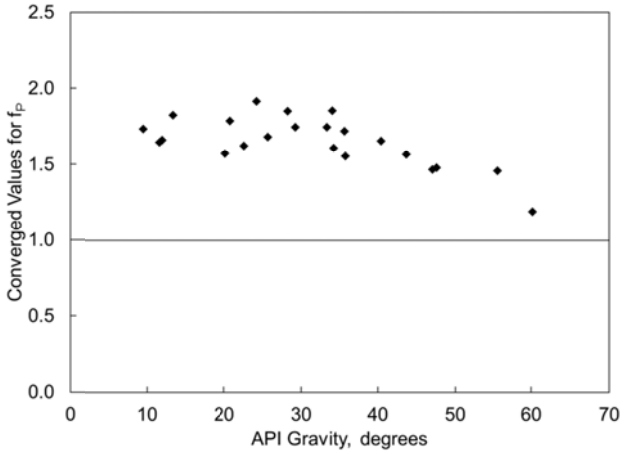

Figure 6. The converged f_P values for the 22 different oils in Table 1. The regression algorithm (Fig. A.2) starts with f_P =1.0, and searches for an optimum f_P in the increasing direction. Perturbation of f_P from 1.0 qualitatively represents deviation of a plus fraction from a n-alkane mixture.

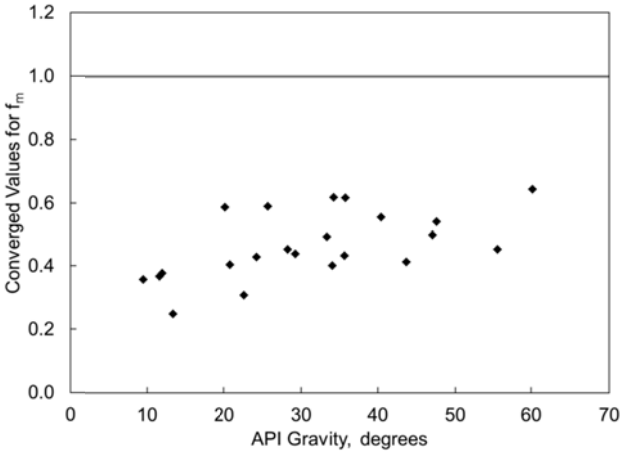

Figure 7. The converged f_m values for the 22 different oils in Table 1. The regression algorithm (Fig. A.2) starts with f_m based on Eq. 7, and searches for an optimum f_m in the increasing direction. Perturbation of f_m from 1.0 qualitatively represents deviation of a plus fraction from a n-alkane mixture.

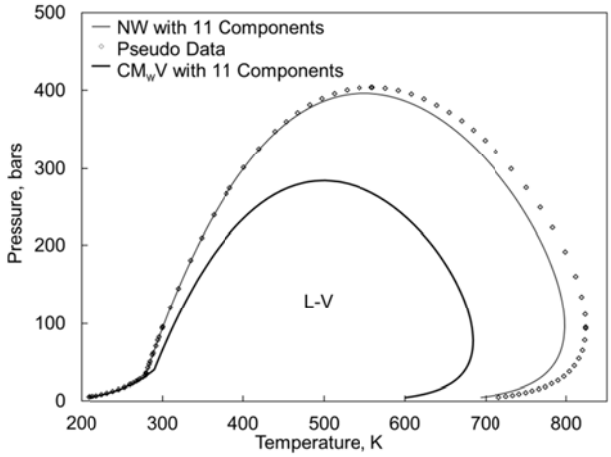

Figure 8. Two-phase P-T diagrams for a mixture of oil 6 10% and C_2 90% based on the new characterization method (NM) and the conventional characterization method with volume-shift parameters (CM_wV). The 11-component models for oil 6 are given in Tables 4 and 5. The pseudo data are generated using the conventional method without using volume shift parameters ($CM_{w/o}V$) with 30 components.

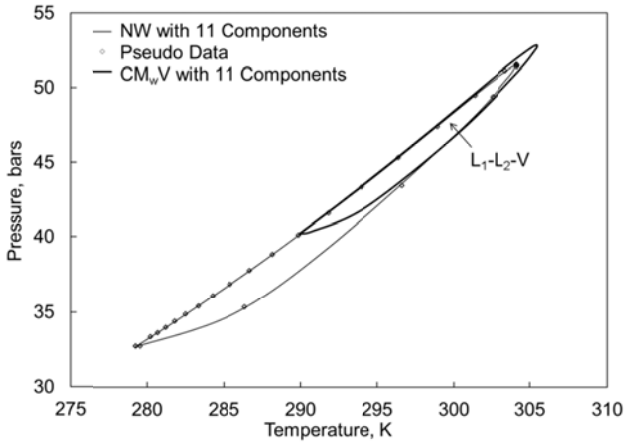

Figure 9. Three-phase P-T diagrams for a mixture of oil 6 10% and C_2 90% based on the NM and the CM_wV. The 11-component models for oil 6 are given in Tables 4 and 5. The pseudo data are generated using the $CM_{w/o}V$ with 30 components.

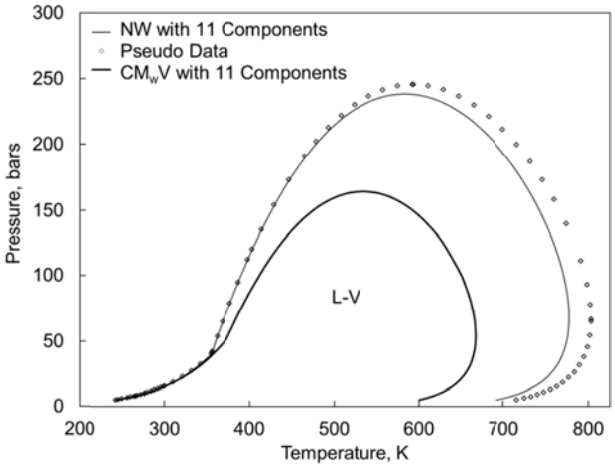

Figure 10. Two-phase P-T diagrams for a mixture of oil 6 10% and C_3 90% based on the NM and the CM_wV. The 11-component models for oil 6 are given in Tables 4 and 5. The pseudo data are generated using the $CM_{w/o}V$ with 30 components.

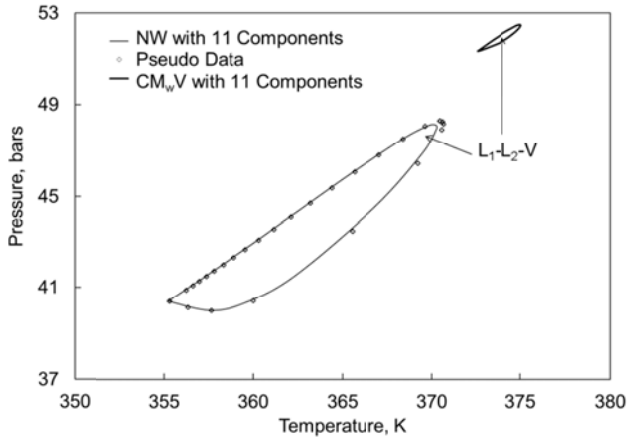

Figure 11. Three-phase P-T diagrams for a mixture of oil 6 10% and C_3 90% based on the NM and the CM_wV. The 11-component models for oil 6 are given in Tables 4 and 5. The pseudo data are generated using the $CM_{w/o}V$ with 30 components.

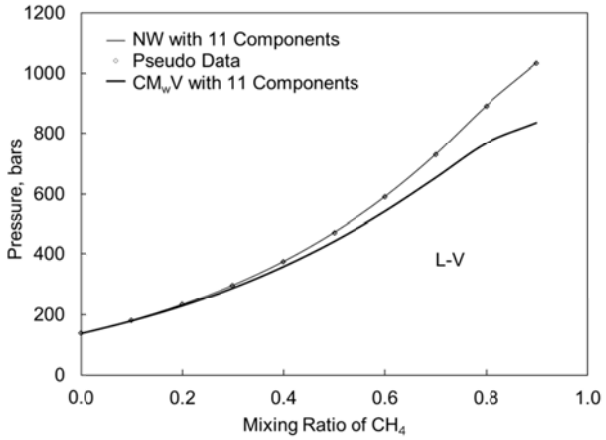

Figure 12. P-x diagrams for the oil-6/C_1 pseudo binary pair at 333.15 K based on the NM and CM_wV with 11 components. The 11-component models are given in Tables 4 and 5. The pseudo data are generated using the $CM_{w/o}V$ with 30 components.

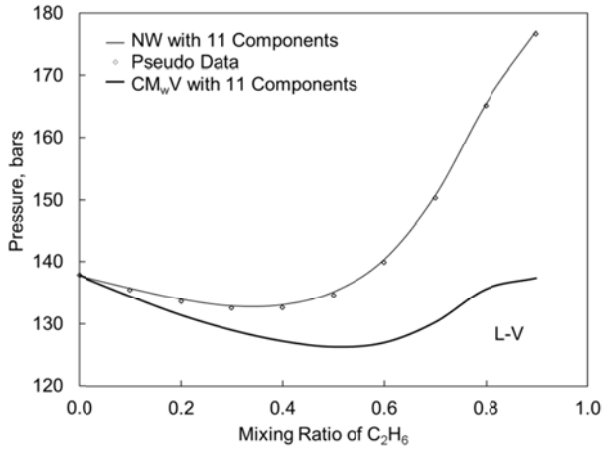

Figure 13. P-x diagrams for the oil-6/C_2 pseudo binary pair at 333.15 K based on the NM and CM_wV with 11 components. The 11-component models are given in Tables 4 and 5. The pseudo data are generated using the $CM_{w/o}V$ with 30 components.

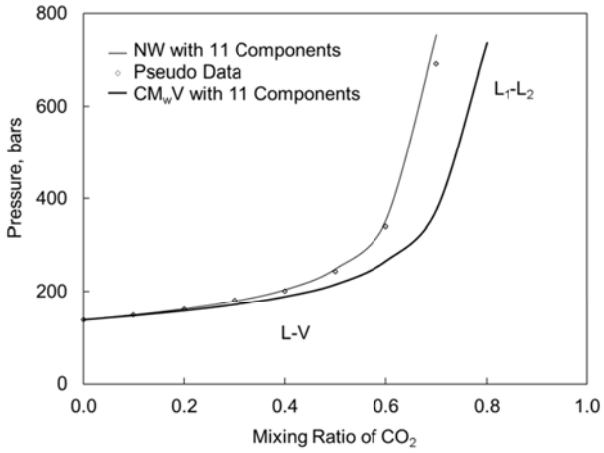

Figure 14. P-x diagrams for the oil-6/CO_2 pseudo binary pair at 333.15 K based on the NM and CM_wV with 11 components. The 11-component models are given in Tables 4 and 5. The pseudo data are generated using the $CM_{w/o}V$ with 30 components.

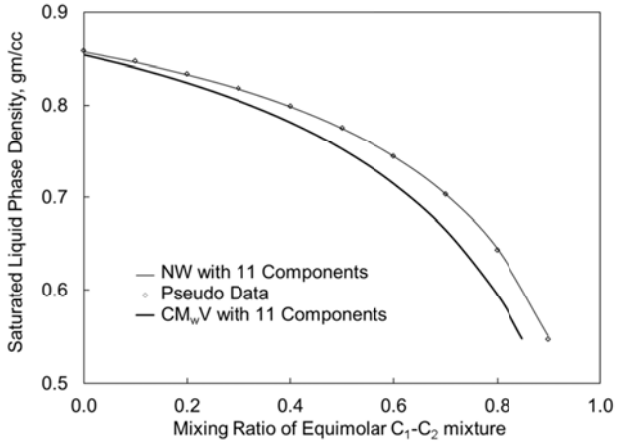

Figure 15. Saturated liquid densities for mixtures of oil 6 and the equimolar C_1-C_2 mixture at 333.15 K. The 11-component models based on the NW and the CM_wV are given in Table 4 and 5, respectively. The pseudo data are generated using the $CM_{w/o}V$ with 30 components.

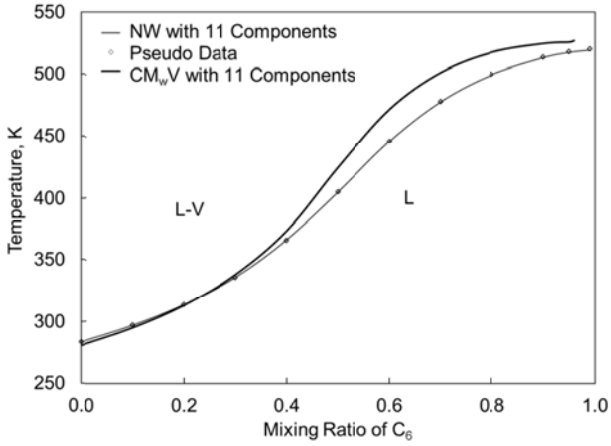

Figure 16. T-x diagrams for the oil-3/C_6 pseudo binary pair at 34.47 bars. The 11-component models based on the NW and the CM_wV are given in Table 2 and 3, respectively. The pseudo data are generated using the $CM_{w/o}V$ with 30 components.

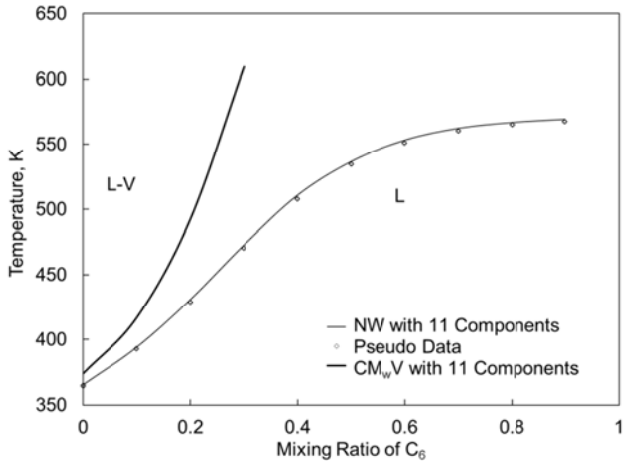

Figure 17. T-x diagrams for the oil-3/C_6 pseudo binary pair at 60.00 bars. The 11-component models based on the NW and the CM_wV are given in Table 2 and 3, respectively. The pseudo data are generated using the $CM_{w/o}V$ with 30 components.

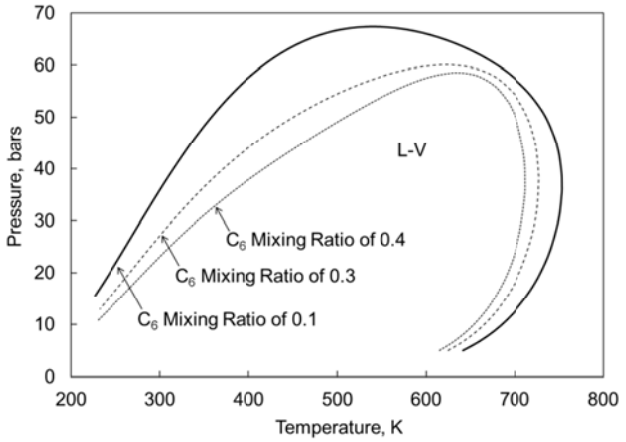

Figure 18. Two-phase PT diagrams for mixtures of oil 3 and C_6 at four different C_6 mixing ratios, 0.1, 0.3, and 0.4. At the C_6 mixing ratio of 0.4, there is no two-phase region at 60.0 bars, which can be also seen in Fig. 17.

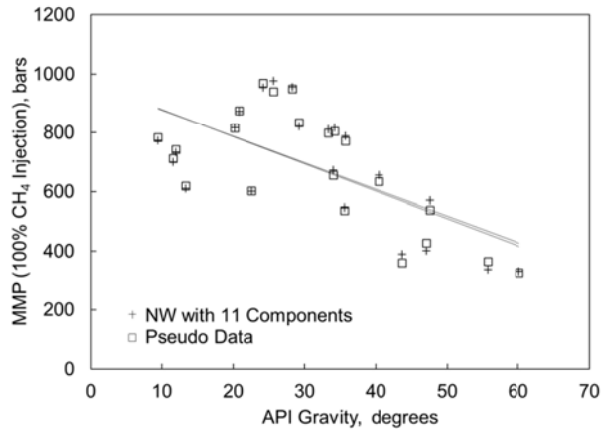

Figure 19. Comparison of MMP calculations for 18 oils in Table 1 based on the NM with 11 components and the $CM_{w/o}V$ with 30 components. The injection gas is pure methane. The MMPs for 18 oils are calculated at their own reservoir temperatures, which are different from one another. The two trend lines for the NW with 11 components and the $CM_{w/o}V$ with 30 components almost overlap each other.

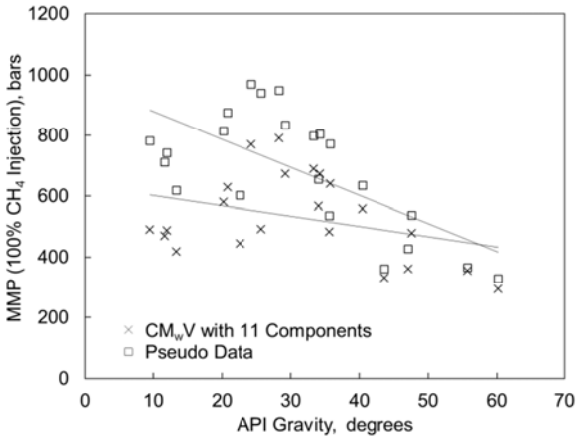

Figure 20. Comparison of MMP calculations for 18 oils in Table 1 based on the CM_wV with 11 components and the $CM_{w/o}V$ with 30 components. The injection gas is pure methane. The MMPs for 18 oils are calculated at their own reservoir temperatures, which are different from one another. The two trend lines for the CM_wV with 11 components and the $CM_{w/o}V$ with 30 components deviate from each other as the API gravity becomes smaller.

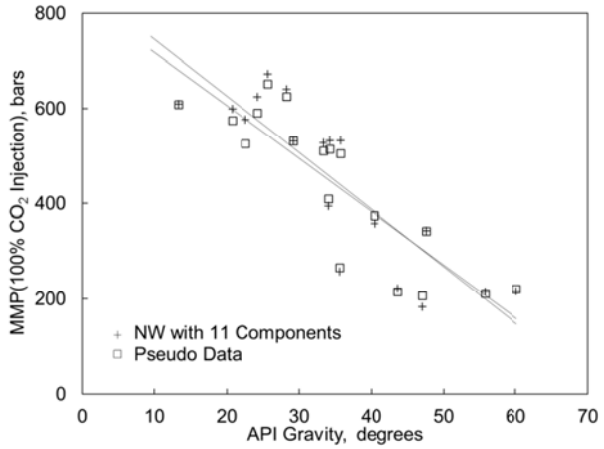

Figure 21. Comparison of MMP calculations for 18 oils in Table 1 based on the NM with 11 components and the $CM_{w/o}V$ with 30 components. The injection gas is pure CO_2. The MMPs for 18 oils are calculated at their own reservoir temperatures, which are different from one another. The two trend lines for the NW with 11 components and the $CM_{w/o}V$ with 30 components are close to each other.

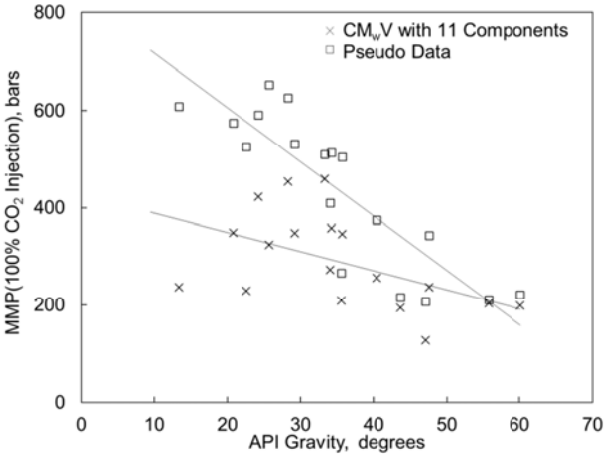

Figure 22. Comparison of MMP calculations for 18 oils in Table 1 based on the CM_wV with 11 components and the $CM_{w/o}V$ with 30 components. The injection gas is pure CO_2. The MMPs for 18 oils are calculated at their own reservoir temperatures, which are different from one another. The two trend lines for the CM_wV with 11 components and the $CM_{w/o}V$ with 30 components deviate from each other as the API gravity becomes smaller.

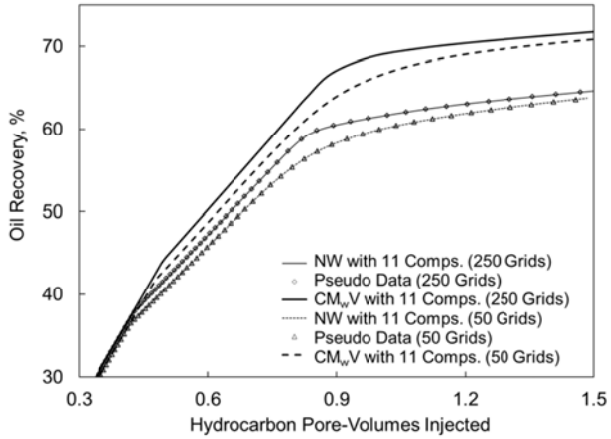

Figure 23. Oil recovery predictions in 1-D oil displacement simulations based on the NM and CM_wV with 11 components, along with pseudo data points generated from the $CM_{w/o}V$ with 30 components. Oil 6 is displaced by the equimolar C_1/C_2 mixture at 333.15 K at 200 bars, which is below MMP. Input parameters are given in Table 6. The recovery curves for 0.0-0.3 HCPVI nearly coincide, and they are not shown.

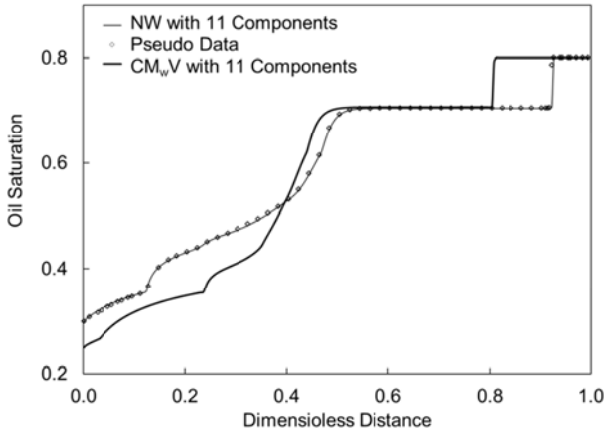

Figure 24. Oil saturation profiles at 0.4 HCPVI for the oil-6 displacement with the equimolar C_1/C_2 mixture at 333.15 K and 200 bars. Predictions using the NM and CM_wV with 11 components are shown along with pseudo data generated from the $CM_{w/o}V$ with 30 components.

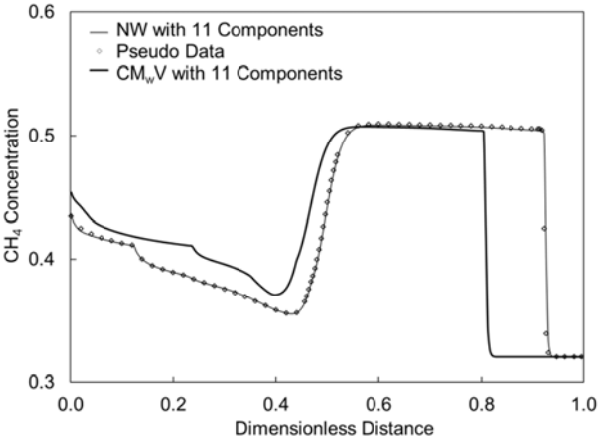

Figure 25. Concentration profiles for C_1 at 0.4 HCPVI for the oil-6 displacement with the equimolar C_1/C_2 mixture at 333.15 K and 200 bars. Predictions using the NM and CM_wV with 11 components are shown along with pseudo data generated from the $CM_{w/o}V$ with 30 components.

Appendix-A

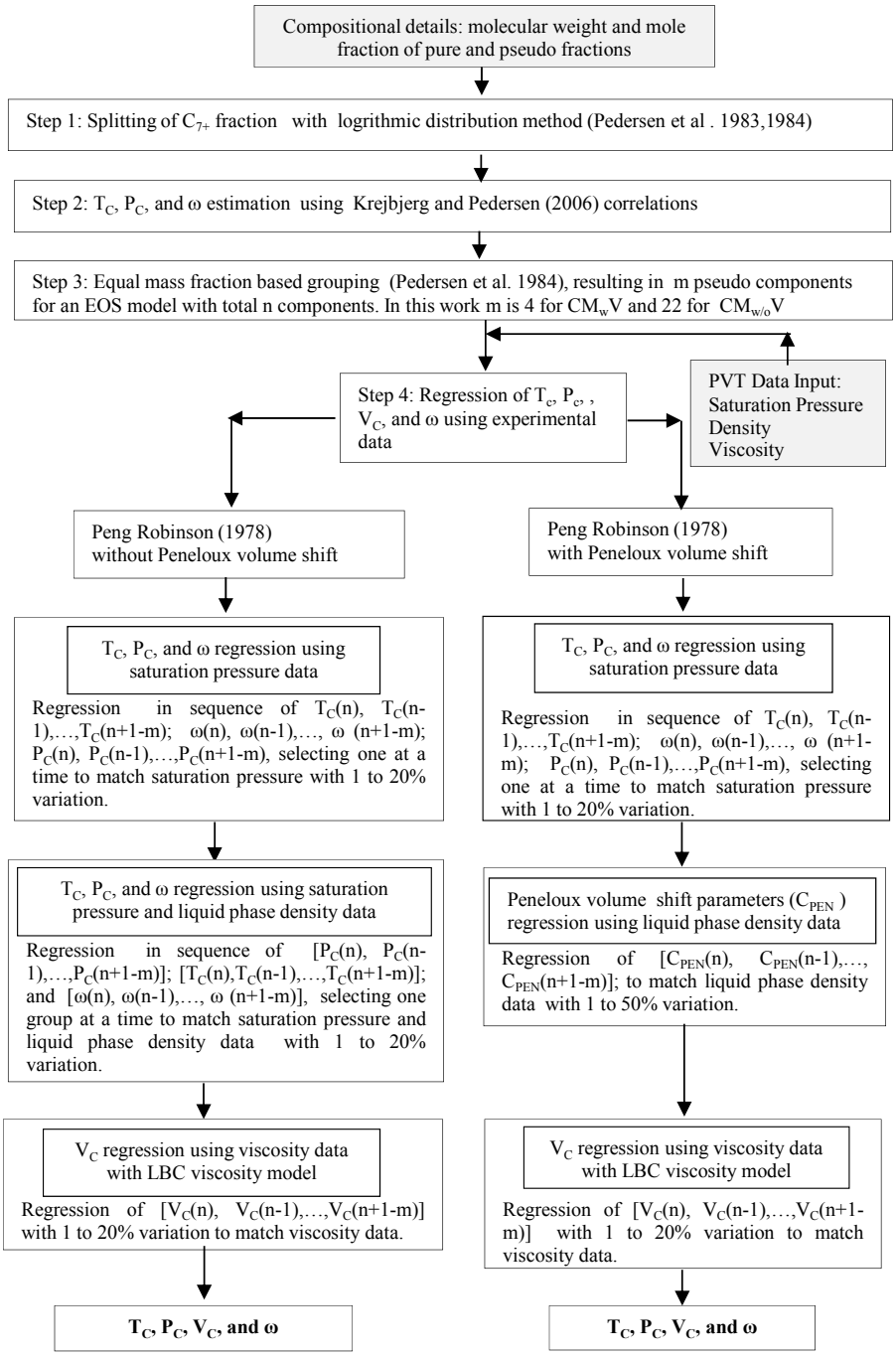

Figure A.1. Flow chart for the conventional characterization method (CM) in this research, which is based on Pedersen and Christensen (2007). The shaded blocks show the input data. For the fluids used in this research, P_{SAT}, density, and viscosity data are used for parameter regression. The CM with volume-shift parameters is referred to as the CM_wV (the right branch of the flow chart). The $CM_{w/o}V$ is the CM without volume-shift parameters (the left branch of the flow chart). See the Introduction section for the definitions of steps 1-4.

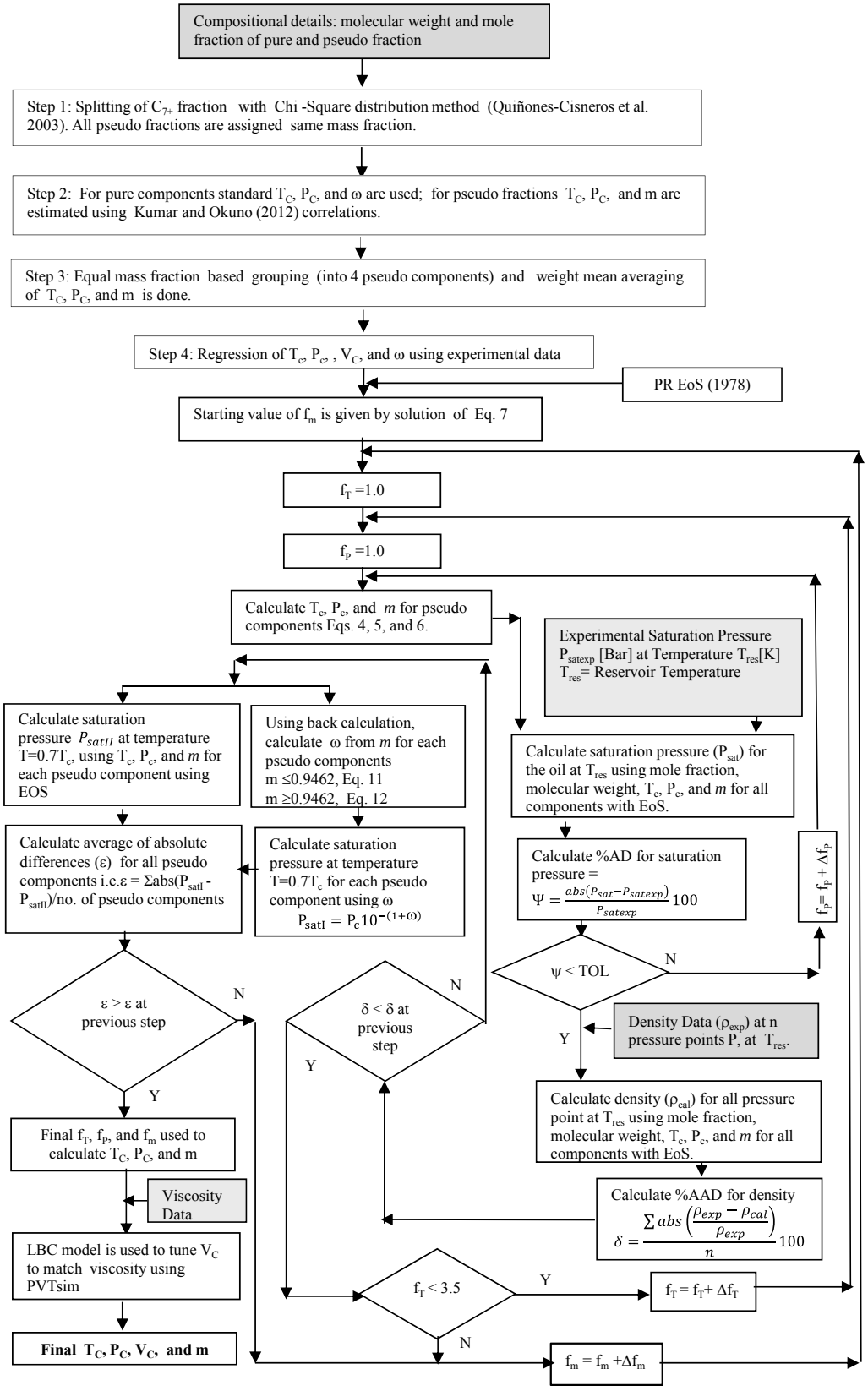

Figure A.2. Flow chart for the new characterization method (NM) developed in this research. The shaded blocks show the input data. For the fluids used in this research, P_{SAT}, density, and viscosity data are used for parameter regression.